JOURNAL OF GEOPHYSICAL RESEARCH, VOL. 104, NO. A12, PAGES 28,361–28,378, DECEMBER 1, 1999

A numerical study of solar wind – magnetosphere interaction for northward interplanetary magnetic field

P. Song, D.L. DeZeeuw, T.I. Gombosi, and C. P. T. Groth

Space Physics Research Laboratory, Department of Atmospheric, Oceanic and Space Sciences, University of Michigan, Ann Arbor

K.G. Powell

Department of Aerospace Engineering, University of Michigan, Ann Arbor

Abstract. The solar wind–magnetosphere interaction for northward interplanetary magnetic field (IMF) is studied using a newly developed three-dimensional adaptive mesh refinement (AMR) global MHD simulation model. The simulations show that for northward IMF the magnetosphere is essentially closed. Reconnection between the IMF and magnetospheric field is limited to finite regions near the cusps. When the reconnection process forms newly closed magnetic field lines on the dayside, the solar wind plasma trapped on these reconnected magnetic field lines becomes part of the low-latitude boundary layer (LLBL) plasma and it convects to the nightside along the magnetopause. The last closed magnetic field line marks the topological boundary of the magnetospheric domain. When the last closed magnetic field line disconnects at the cusps and reconnects to the IMF, its plasma content becomes part of the solar wind. Plasma convection in the outer magnetosphere does not directly contribute to the reconnection process. On the dayside the topological boundary between the solar wind and the magnetosphere is located at the inner edge of the magnetopause current layer. At the same time, multiple current layers are observed in the high-altitude cusp region. Our convergence study and diagnostic analysis indicate that the details of the diffusion and the viscous interaction do not play a significant role in controlling the large-scale configuration of the simulated magnetosphere. It is sufficient that these dissipation mechanisms exist in the simulations. In our series of simulations the length of the magnetotail is primarily determined by the balance between the boundary layer driving forces and the drag forces. With a parametric study, we find that the tail length is proportional to the magnetosheath plasma beta near the magnetopause at local noon. A higher solar wind density, weaker IMF, and larger solar wind Mach number results in a longer tail. On the nightside downstream of the last closed magnetic field line the plasma characteristics are similar to that in the magnetotail, posing an observational challenge for identification of the topological status of the corresponding field lines.

1. Introduction

The steady state topology of the magnetosphere for due south and north pointing interplanetary magnetic field (IMF) conditions is of great theoretical interest for magnetospheric physics. In an idealized situation (assuming a nonrotating planet with a strictly southward pointing magnetic dipole moment) such configurations exhibit two planes of symmetry (the equatorial plane and the noon-midnight meridian). The due south and north IMF configurations have been the subjects of countless investigations starting with the seminal paper by *Dungey* [1961].

Paper number 1999JA900378.
0148-0227/99/1999JA900378$09.00

When the IMF is strictly northward, it is parallel to the Earth's dipole magnetic field. *Dungey* [1961] proposed that reconnection between the IMF and the magnetospheric field can take place at certain points along the nightside magnetopause. In the *Dungey* [1961] model the magnetosphere is closed except at the two reconnection points. In his pioneering work, *Dungey* [1961] concentrated on the global magnetospheric configuration and he did not provide the ionospheric convection pattern (even though he did consider ionospheric convection patterns for southward IMF).

Many of the later models for northward IMF have assumed that the magnetosphere is open. One of the difficulties for an open magnetospheric model for northward IMF is that it is difficult to disconnect the magnetospheric field from the IMF in the distant tail (we note that for southward IMF, the two magnetic fields become disconnected through nightside reconnection). In order to solve this problem, some of

these models invoked either a finite B_y component [*Russell*, 1972; *Reiff and Burch*, 1985; *Burch et al.*, 1992] or a finite B_x component [*Kan and Burke*, 1985; *Crooker*, 1992] (both of which break the symmetry of the configuration) or require quite complicated magnetic field geometries, while others did not provide a complete three dimensional configuration.

Recently, *Song et al.* [1999] proposed a closed magnetosphere model for due northward IMF, which is globally consistent with the *Dungey* [1961] reconnection model. It provides a self-consistent framework encompassing not only magnetospheric convection but also reverse ionospheric convection cells and the northward B_z (NBZ) currents [*Burke et al.*, 1979; *Iijima et al.*, 1984; *Zanetti et al.*, 1984; *Clauer and Friis-Christensen*, 1988; *Taguchi and Hoffman*, 1996]. These features are often difficult to model self-consistently in open magnetosphere models. One of the important elements of the *Song et al.* [1999] model is the recognition that distant closed magnetic field lines can move tailward instead of earthward in the presence of cusp reconnection.

The interaction between the magnetosphere and a purely northward IMF has also been investigated numerically. *Ogino and Walker* [1984] were the first to show reconnection in the cusp regions. However, owing to the limitation of the simulation domain, the distant tail could not be resolved well. The dayside convection in the equatorial plane obtained by *Ogino and Walker* [1984] is consistent with the simulation results of the present study. Another early simulation model for northward IMF was presented by *Wu* [1985]. In his simulation an X-type geometry is formed at each cusp region, although *Wu* [1985] suggested that it is a neutral point and not a reconnection point. Nevertheless, the simulations indicated that the magnetosphere is closed and the length of the tail decreases as B_z varies from zero to a finite positive value. This tendency is also consistent with the simulations shown in the present work.

Nearly a decade later, *Usadi et al.* [1993] presented a simulation model with a spatial computational domain much larger than the ones used by the early models. These results again showed a closed magnetosphere for northward IMF, with reconnection taking place in the cusp regions. *Usadi et al.* [1993] also confirmed that the magnetotail becomes shorter as the northward IMF increases from zero. In addition, the flow in the equatorial plane in the distant tail shows both earthward and tailward convection, although the flow pattern becomes noisier as the simulation time increases.

More recently, *Fedder and Lyon* [1995] and *Mobarry et al.* [1996] published the results obtained from a significantly improved model. It includes a much larger simulation domain, improved ionospheric boundary conditions, and a high-resolution upwind numerical scheme. In addition to the features shown in previous models, such as cusp reconnection and closed magnetosphere, the results also showed NBZ currents, ionospheric reverse convection cells, and a flow divergence in the equatorial plane near 95 R_E from the Earth in the midnight. Among the major differences between these results and those presented in our paper are a much longer tail (the length of the tail is 155 R_E, while the entire magnetosphere is 165 R_E long), very small LLBL/tail region in the distant tail region, and more complicated ionospheric currents [*Fedder and Lyon*, 1995; *Mobarry et al.*, 1996].

Results from another recent simulation model were presented by *Berchem et al.* [1995] and *Raeder et al.* [1995]. Similar to other models, this model also showed cusp reconnection. Distinct from other models, however, in this model the magnetosphere is never fully closed. Simulations for all IMF conditions started with a late-time solution for southward IMF. An X-line type reconnection continues in the near Earth magnetotail current sheet, even hours after the IMF was turned from south to north. A channel of a few Earth radii wide is formed and persists at the center of the magnetotail linking near the Earth magnetotail reconnection region to the solar wind. The simulation results depend on initial conditions. If the simulation starts with a northward IMF, the magnetosphere would be closed [*Raeder*, 1998]. No ionospheric convection pattern was provided in these papers [*Berchem et al.*, 1995; *Raeder et al.*, 1995].

Using yet another magnetosphere model R. M. Winglee and R. K. Elsen (unpublished manuscript 1995) made several runs with due northward IMF but different dynamic pressure and magnitude of the IMF. In these runs the period of steady northward IMF lasted 1 to 2 hours. On the basis of these simulations, R. M. Winglee and R. K. Elsen (unpublished manuscript, 1995) concluded that for $B_z \geq 5$ nT the length of the tail continuously shrinks as long as the due northward IMF is maintained. Eventually, short magnetotail configurations were attained.

Gombosi et al. [1998] have recently published a series of magnetosphere simulations with steady northward IMF conditions. These simulations showed closed magnetospheric configurations with cusp reconnection. One of the interesting results of their parametric study was the relationship that the length of the last closed magnetospheric field line (the tail) varies as $1/B_z$ for northward IMF conditions [*Gombosi et al.*, 1998].

The present work uses the MHD numerical model developed at the University of Michigan [*Gombosi et al.*, 1998] to provide more detailed account of the processes described and required in the model of *Song et al.* [1999]. Here we concentrate on the physical understanding of simulation results. In section 2, we briefly describe the numerical scheme used in the simulations. In section 3, we discuss the results of simulations and their physical implications. Then, in section 4, we focus on the coupling processes between the solar wind and magnetosphere. Specific topics discussed include the magnetopause, the formation of the LLBL, and the length of the magnetotail.

2. Numerical Solution of Ideal MHD Equations

2.1. Description of BATS-R-US

The code used in this study employs a Block Adaptive-Tree Solar-wind Roe-type Upwind Scheme (BATS-R-US). It solves the governing equations of ideal magnetohydrodynamics, which are written in conservation form as

$$\frac{\partial \mathbf{U}}{\partial t} + (\nabla \cdot \mathbf{F})^{\mathrm{T}} = \mathbf{S}_B\,, \tag{1}$$

where the eight dimensional solution and source vectors $\mathbf{U}$ and $\mathbf{S}_B$ are given by

$$\mathbf{U} = \begin{bmatrix} \rho \\ \rho\mathbf{u} \\ \mathbf{B} \\ \epsilon \end{bmatrix} \quad \mathbf{S}_B = -\begin{bmatrix} 0 \\ \mathbf{B} \\ \mathbf{u} \\ \mathbf{u}\cdot\mathbf{B} \end{bmatrix} \nabla \cdot \mathbf{B}\,. \tag{2}$$

We note that the source term $\mathbf{S}_B$ arises solely from the Galilean invariant form of Faraday's law [*Jackson*, 1975]. It equals zero when the magnetic field is divergence free and the conventional form of ideal MHD equations is recovered. The divergence-free condition can be easily specified in the solar wind, and it then convects into the simulation domain according to the conservation of the divergence of the magnetic field which is obtained by taking the divergence of the third equation in equation (1). Finally, $\mathbf{F}$ is a flux tensor having the form

$$\mathbf{F} = \begin{bmatrix} \rho\mathbf{u} \\ \rho\mathbf{u}\mathbf{u} + \left(p + \frac{1}{2\mu_0}B^2\right)\mathbf{I} - \frac{1}{\mu_0}\mathbf{B}\mathbf{B} \\ \mathbf{u}\mathbf{B} - \mathbf{B}\mathbf{u} \\ \mathbf{u}\left(\epsilon + p + \frac{1}{2\mu_0}B^2\right) - \frac{1}{\mu_0}(\mathbf{B}\cdot\mathbf{u})\,\mathbf{B} \end{bmatrix}^{\mathrm{T}}, \tag{3}$$

where the total plasma energy density ϵ is given by

$$\epsilon = \frac{1}{2}\rho u^2 + \frac{p}{\gamma - 1} + \frac{1}{2\mu_0}B^2\,, \tag{4}$$

and γ and μ_0 are the ratio of specific heats and the permeability in vacuum, respectively. Represented in the equation set are four equations for the conservation of mass, momentum, and total plasma energy, as well as the induced electric field as described by Faraday's law. The variables ρ, $\mathbf{u}$, p, and $\mathbf{B}$ correspond to the density, velocity, pressure, and magnetic field, respectively.

We describe briefly here the BATS-R-US code. A detailed description of the code can be found in the work of *Powell et al.* [1999]. In this code, the hydrodynamic and electromagnetic effects are solved in a fully three-dimensional tightly coupled manner, rather than in separate steps [*Gombosi et al.*, 1996; *Powell et al.*, 1995, 1999]. The tight coupling between the hydrodynamic and electromagnetic quantities makes the scheme work equally well across a range of several orders of magnitude in plasma β where β is the ratio of the thermal and magnetic pressures. A high-resolution finite volume solution upwind scheme is used based on two accurate approximate Riemann solvers, *Roe*'s [1981] scheme [*Powell*, 1994] and *Linde*'s [1998] solver. The code uses a limited reconstruction that ensures second-order accuracy away from discontinuities, while simultaneously providing the stability that ensures to maintain nonoscillatory solutions.

The basic data structure used in the BATS-R-US approach is an adaptive-blocks scheme [*Powell et al.*, 1999]. Each block is a Cartesian grid of cells, and all blocks are identical in structure. Adaptive blocks partition space into regions according to the gradients in solutions of physical quantities. In a region where large gradients exist, the resolutions will need to be refined. The block is replaced by eight child subblocks (one for each octant of the parent block). Likewise, if coarsening is needed, the eight children are replaced by a parent block. The blocks in the grid, at their various levels of refinement, are stored in a tree-like data structure.

BATS-R-US was specially designed to handle objects with strong intrinsic magnetic fields. In this case, there is often a large spatial gradient associated with the intrinsic magnetic field. The scheme solves for only the deviation of the magnetic field from the intrinsic magnetic field, namely, $\mathbf{B}_1 = \mathbf{B} - \mathbf{B}_o$, where $\mathbf{B}_o$ is the intrinsic magnetic field corresponding to a dipole magnetic field with a strength of 0.31 G at the equatorial surface of the Earth. We note that in this formulation $\mathbf{B}_1$ does not have to be small; therefore this decomposition is completely general.

2.2. Boundary Conditions

At the upstream boundary a free streaming solar wind enters the computational domain. The other five outer boundaries contain free-streaming solar wind conditions. Since these boundaries are far enough away so that the plasma flow is supersonic and superalfvénic at these locations, the effects of the boundary conditions on the solutions are minimal.

The inner boundary of the simulation domain is at 3 R_E. At the inner boundary the boundary conditions allow no mass flux across the boundary. Reflective boundary conditions are used for the mass density and thermal pressure. Neumann conditions are applied to the tangential components of the deviative magnetic field (the difference between the dipole magnetic field and the actual magnetic field) and Dirichlet condition for the normal component. The velocity at the inner boundary is specified by the coupling with the ionosphere as to be discussed below.

The coupling between the magnetosphere and the ionosphere is taken into account in a conventional way. It assumes that magnetospheric field-aligned currents flow from the magnetospheric inner boundary into a height-integrated electrostatic ionosphere. Under MHD conditions, $\nabla \cdot \mathbf{j} = 0$. This means that the normal component of the magnetospheric current j_n at the interface between the magnetosphere and ionosphere (i.e., the current that downward enters the ionosphere from the magnetosphere is positive) must be diverted into horizontal currents in the height-integrated thin ionosphere. With the help of Ohm's law applied in the ionsphere at R_0 this can be written as

$$j_n\,(R_0, \theta, \phi) = -\left[\nabla_t \cdot (\Sigma \cdot \nabla\psi)_t\right]_{r=R_0}\,, \tag{5}$$

where ψ is the ionospheric electrostatic potential and Σ is the height integrated conductivity tensor. The symbol ∇_t denotes the tangential component of the gradient operator in the ionosphere surface, the subscript "t" refers to the tangen-

tial components at the magnetospheric boundary, and θ and ϕ denote latitude and longitude, respectively. Once the ionospheric electrostatic potential is derived, it is mapped along the magnetic field lines to the magnetospheric inner boundary assuming the magnetic field lines to be equipotential. One can then calculate the convection velocity, $\mathbf{u}_i$:

$$\mathbf{u}_i = \left(\frac{\mathbf{B}_i \times \nabla \psi}{B_i^2} \right)_t, \tag{6}$$

where the subscript "i" denotes the values at the inner boundary. This convection velocity is used as the boundary condition for the magnetospheric simulation. This procedure has been summarized by *Goodman* [1995], whose results were modified by *Amm* [1996]. In the present simulation we solved the equations given by *Amm* [1996].

2.3. Simulation Parameters

The solar wind and terrestrial parameters used in the present simulations are based on the community reference benchmark suite. The elements of the ionospheric conductance tensor are constant in time and spatially uniform ($\Sigma_P = 5$ S, $\Sigma_H = 0$ S, $\Sigma_0 = 5000$ S, where Σ_P, Σ_H, and Σ_0 are ionospheric Pedersen, Hall, and field-aligned conductances, respectively. The specific heat ratio is 5/3. The reference run uses an undisturbed solar wind velocity $u = 400$ km/s, density $n = 5$ cm^{-3}, and acoustic Mach number of 8. The interplanetary magnetic field is 5 nT and due north.

The computational domain extends from $x = 192\ R_E$ to $x = -384\ R_E$ along the Sun-Earth line and from -192 to 192 R_E in the y and z directions. The smallest computational cell is $0.125 \times 0.125 \times 0.125\ R_E^3$ and six levels of refinement are used. The total number of computational cells is around 1 million. The height-integrated electrostatic ionosphere is located on a spherical surface with a radius of 1.08 R_E.

The code has been carefully validated for northward IMF runs. The validation studies have been presented in an earlier paper [*Gombosi et al.*, 1998]. Here we only mention that the solutions are grid converged and all steady state solutions are independent of the initial conditions.

3. Results: Qualitative Analysis

Plate 1 shows results of our reference run. The results presented are the steady state solution. This result can be obtained from either northward IMF and southward IMF as the initial condition. The dynamic processes from the initial conditions to the steady state solutions seem to follow a large scale monotonic evolution. Little evidence for turbulence or bursty bulk flows, such as those reported by *Angelopoulos et al.* [1994], has been observed. The solar wind input parameters used are as described in the last section. Later in the paper we will discuss results of simulation runs with different input parameters. These runs will be used to examine the global magnetospheric response to different solar wind conditions.

Plate 1a shows the noon-midnight meridian for the northern hemisphere. The white lines with arrowheads are magnetic field lines. The color coding represents the logarithm of the thermal pressure. The thick red lines indicate topological boundaries which separate flows of distinct characteristics. Plate 1b shows the equatorial plane for the morningside. White lines with arrowheads are streamlines and the color coding represents the sonic Mach number.

It can be seen in Plate 1 that a bow shock is formed in front of the magnetosphere. This fast magnetosonic shock decelerates, deflects, and heats the solar wind plasma. The magnetosphere is essentially closed with the exception of a small region near the cusp where reconnection takes place between the IMF and the magnetospheric field.

3.1. Planes of Symmetry

The simulation results are presented on three surfaces: the equatorial and noon-midnight meridian planes and the height-integrated ionosphere (see Plate 2). Both the equatorial and the noon-midnight planes are planes of symmetry for the particular situation considered in this paper. This means that the solution must exhibit certain properties in these planes.

In the noon-midnight meridian plane, both the magnetic field and the velocity have no component normal to the plane. As discussed in the last section, in the magnetosphere, the governing equations are ideal MHD. In ideal MHD, the magnetic field lines and streamlines are equipotentials because the electric field is perpendicular to both magnetic field and velocity. The magnetic field lines in the noon-midnight meridian plane can be of the same potential if they are on the same streamline. The red thick lines in Plate 1a separate regions of different flows and hence regions of different potentials.

For symmetry reasons the magnetic field has no component in the equatorial plane, therefore the magnetic field is always vertical to the $Z = 0$ plane and points northward everywhere in our case. In contrast, plasma streamlines do not leave the equatorial plane. An immediate consequence of these facts is that the motional electric field is in the equatorial plane and it is normal to the streamlines. The potential difference between two given streamlines in the equatorial plane remains the same throughout the plane. Magnetospheric electric currents are associated with the distortion of the magnetic field from the dipole magnetic field. Stretching of the magnetic field generates currents in the clockwise direction while a compression of the magnetic field results in a counterclockwise current in the equatorial plane. The Lorentz force associated with these currents always tends to restore the dipole magnetic field geometry in the closed magnetic field line region. The divergence or convergence of these currents within the closed magnetic field line region generates the field-aligned currents flowing out of the equatorial plane. These field-aligned currents map into the ionosphere. However, we note that the major component of the current in the equatorial region of the distant tail does not

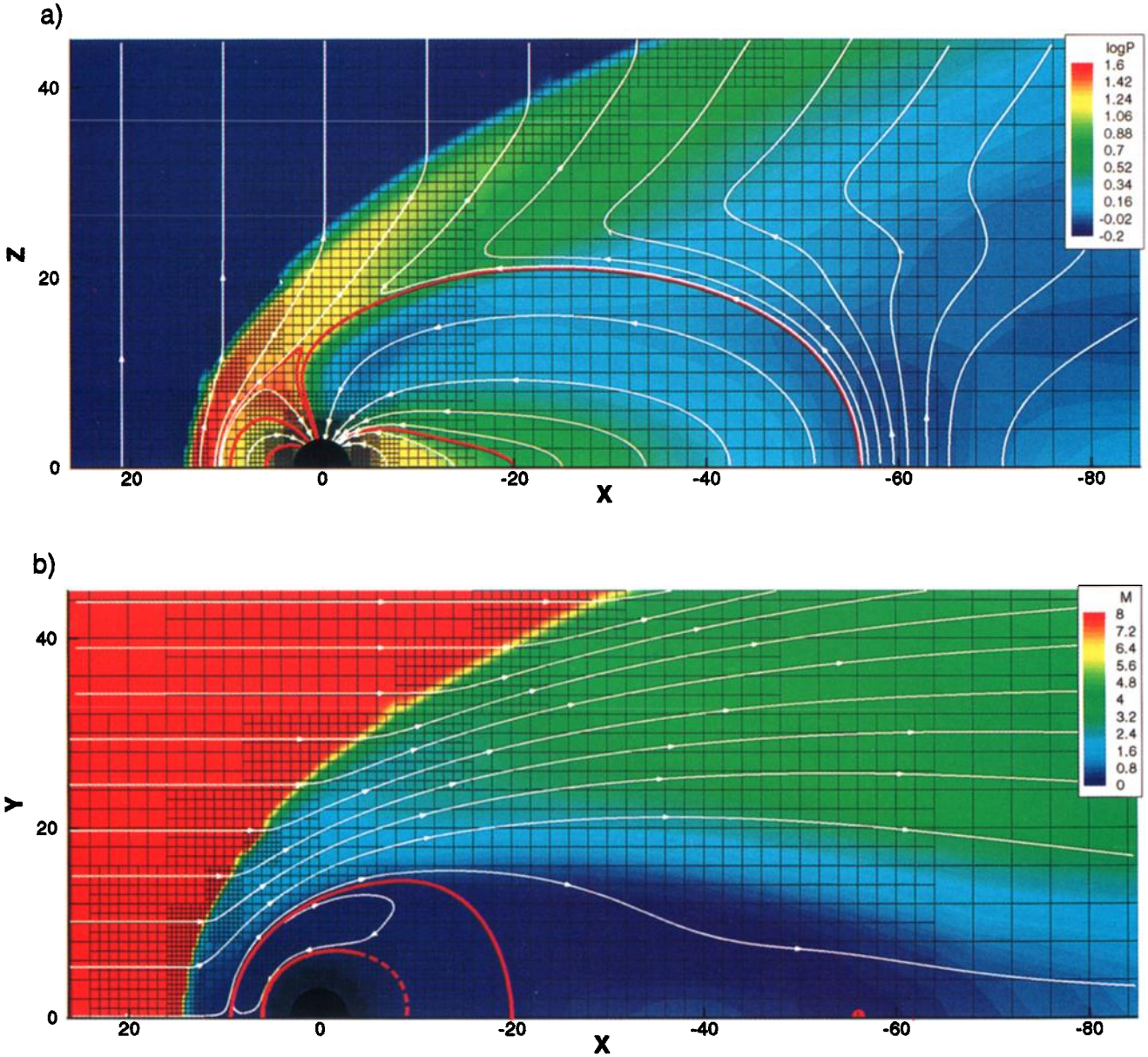

Plate 1. Simulation results for the reference run with northward IMF. The upstream conditions are $n = 5$ cm^{-3}, $u = 400$ km/s, acoustic Mach number $= 8$, specific heat ratio $= 5/3$, and IMF magnitude $= 5$ nT. The two panels are the following: (a) Noon-midnight meridian for the northern hemisphere. The white lines with arrowheads are magnetic field lines. The color coding represents the logarithm of the thermal pressure. The thick red lines indicate the topological boundaries which separate flows of distinct characteristics. (b) Equatorial plane for the morning side. White lines with arrowheads are streamlines and the color coding represents the Mach number. The two red lines indicate the boundaries between distinct flow regions. The dashed segment indicates where streamlines are difficult to define because of the extremely low velocity in the region. The red half-dot indicates the location of the last closed magnetic field line in the midnight.

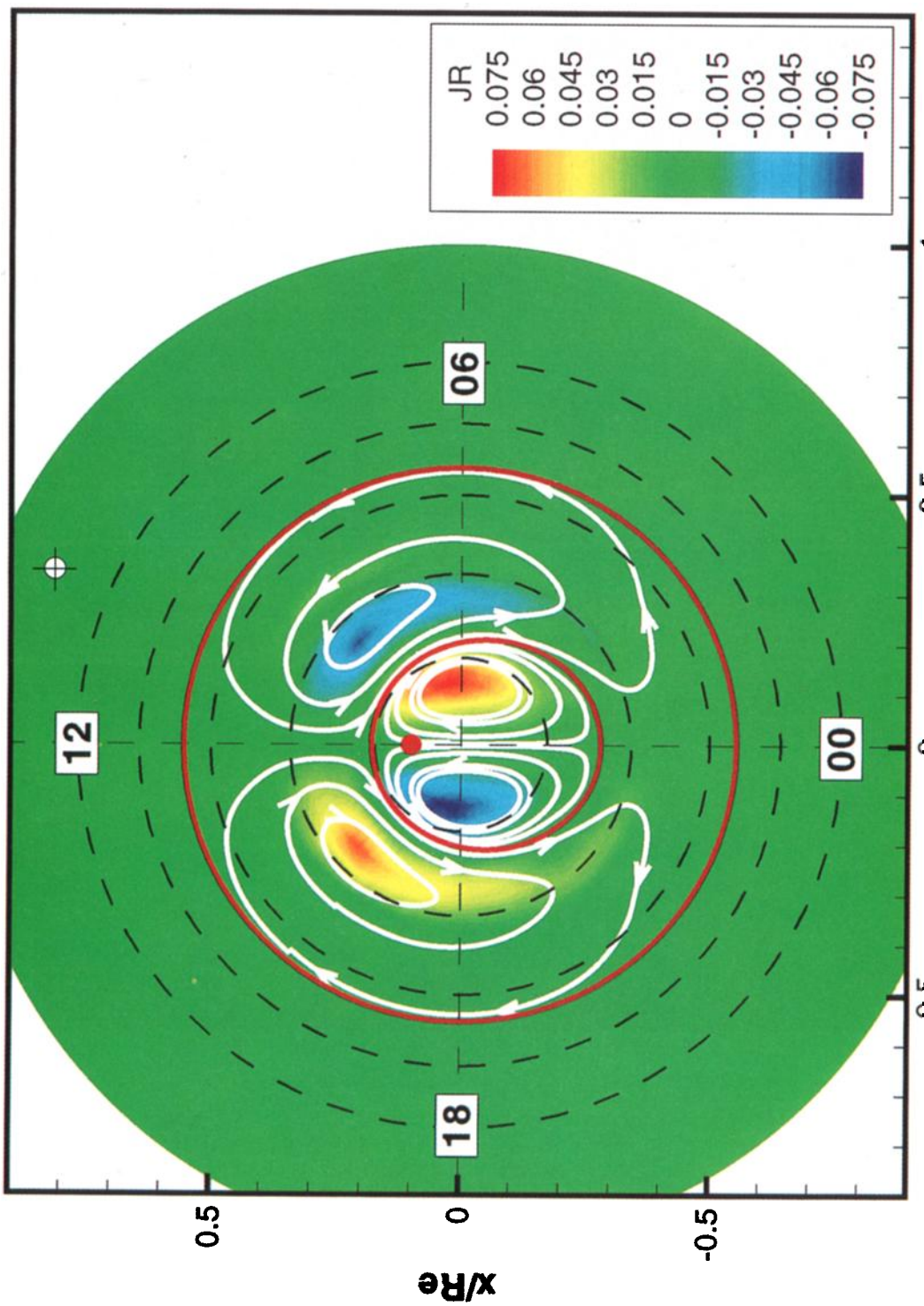

Plate 2. Simulation results for the northern polar ionosphere for the reference run shown in Plate 1. The color code repesents the radial component of the current density with red denoting upward and blue representing downward currents. The white lines with arrowheads are convection streamlines. The thick red circles separate regions of distinct flow characteristics. The red dot indicates the ionospheric footprint of the reconnection point shown in Plate 1a.

converge/diverge within the magnetosphere. It is closed via the "magnetopause" current in the tail region.

3.2. Global Topology and Coupling

Inspection of Plate 1 reveals that there are three topologically distinct regions in the magnetosphere: the inner core or plasmasphere, the outer magnetosphere, and the low-latitude boundary layer (LLBL)/tail region. These regions are separated by boundaries which are marked in Plate 1 by thick red lines. In Plate 1b in a large region, from -10 to $-30R_E$, the flow velocity is very small. Errors in both computation and streamline tracing are significant. Streamlines in this region have not been drawn. However, qualitatively, one can see regions of different flows. The red line near $X = -20\ R_E$ at local midnight is picked up by a change in the Y component of the electric field, which is not shown. The nightside boundary between the plasmasphere and outer magnetosphere cannot be clearly resolved in the simulation. The physics of these regions will be discussed later in this section.

Plate 2 shows the results of the reference run for the height-integrated ionosphere. One can see that three pairs of field-aligned currents connect the magnetosphere and the ionosphere. Closest to the magnetic pole is the pair of NBZ currents, followed by the region I and region II currents as one moves equatorward in the ionosphere. Associated with the NBZ currents is a pair of sunward convection cells in the same sense as the reverse convection cells. Equatorward from the reverse cells is a pair of antisunward convection cells with a sense consistent with viscous convection cells.

The field-aligned currents with the same sense as region II currents shown in Plate 2 must be treated with considerable caution. It should be emphasized that even though our MHD simulation shows a pressure maximum in the ring current region, it is not a realistic ring current, since the model does not include adequately physical processes that generate the ring current. Furthermore, in our present runs, the ionospheric conductances have been assumed to be uniform. Region II currents are so weak that they are not able to drive a separate pair of cells. In reality, an important driver of convection cells associated with region II currents may be the gradients in the conductances, as to be discussed in section 5.4, which are not included in the present runs. In addition, since the dipole magnetic field used in our model is nonrotating, the corotating electric field is not included in the model. We recognize the incomplete nature of our model, and therefore we will not discuss any phenomena associated with region II currents and in the inner magnetosphere in this paper. Moreover, we note that in the absense of realistic region II currents one cannot address the issue of field-aligned current closure in the magnetosphere in any quantitatively consistent manner, since a very important component of the global current system is missing. In spite of the limitations, when used with appropriate caution, global MHD simulations provide important insights into solar wind-magnetosphere coupling processes.

In our simulation model in regions of closed magnetic field lines the forces that directly affect the flow are the pressure gradient force and the Lorentz force. The pressure difference between the subsolar magnetopause and the last closed magnetic field line on the nightside is an important driving force for the plasma flow. This pressure gradient force is further enhanced by the pressure buildup upstream of the dayside magnetopause and the low-pressure region immediately downstream of the last closed magnetic field line in the distant tail, as seen in Plate 1a.

An important feature in an ideal MHD flow is that the motions of different streamlines are related through the induction equation without invoking a viscous force. The electric potential difference between two given streamlines can couple the magnetosphere to the ionosphere and the solar wind along magnetic field lines and can affect plasma transport in these regions. It should be further noticed that this effect is not in the direction of the velocity vector, and hence it can cause shears in the plasma flow. Since in ideal MHD there is no functional relationship between electric field and electric current, they are not necessarily parallel to each other. In regions where they are parallel, the plasma gains energy and the fields lose energy. These regions are sometimes considered analogous to loads in electric circuits. In the regions where the current and electric field are antiparallel, the plasma loses energy and the fields gain energy. These regions are sometimes referred to as dynamos. For example, as shown in Plate 1b, since the magnetic field is northward and the flow in the LLBL/tail region is antisunward, the electric field points dawnward. Because the magnetotail current, which is not shown, is from dawn to dusk, it is antiparallel to the electric field. Therefore the LLBL/tail region functions as a dynamo.

In our model, the governing equation used in the ionosphere is not ideal MHD, but Ohm's law which directly relates the current density to electric fields. There are two major mechanisms that drive the ionospheric plasma: field-aligned currents and electric fields. They operate self-consistently through Ohm's law. Since in our ionospheric model we do not directly solve the momentum equation, the two mechanisms affect the flow in different ways. (1) Field-aligned currents close in the ionosphere through horizontal ionospheric currents. These horizontal currents generate ionospheric electric fields through Ohm's law. In the presence of the Earth's intrinsic magnetic field this electric field causes an $\mathbf{E} \times \mathbf{B}$ drift motion of the plasma. (2) The magnetospheric electric potential maps directly to the ionosphere (since in MHD magnetic field lines are equipotentials). The potential difference between magnetic field lines results in the ionospheric electric field. This ionospheric electric field needs to be consistent with that derived from the field-aligned currents, or additional Petersen currents will be generated and need to be closed in some ways. In addition, when gradients in conductances are allowed, the gradients in the conductances will be built up to modulate the above two processes.

3.3. Interpretation

Plate 3 summarizes our physical understanding of the global convection and mapping patterns in the magnetosphere and ionosphere [*Song et al.*, 1999]. There are three major topological regions in the magnetosphere: the inner core or plasmasphere, the outer magnetosphere, and the LLBL/tail region. These regions are separated by separatrix surfaces. They correspond to the magnetopause, the boundary between the outer magnetosphere and LLBL/tail, and the plasmapause. Under ideal MHD approximation, there is no mass flux across a separatrix surface unless there is a topological change at the surface. The inner two separatrix surfaces are magnetic surfaces. However, because of reconnection at the cusps, the outermost surface, the magnetopause, undergoes a topological change in certain areas. Consequently, the solar wind flux enters through the magnetopause on the dayside and magnetospheric flux exits through the nightside magnetopause.

The LLBL/tail region consists of a pair of convection channels from the subsolar magnetopause to the last closed magnetic field line in the distant tail. The convection in this region is directly driven by the entry of the solar wind plasma. In the ionosphere this region maps to the region within the polar caps. This is the region where one expects precipitation of particles of solar wind origin. Few particles from the steadily trapped magnetospheric population would be observed in the polar cap at ionospheric altitudes. The distortion of the magnetic field in this region generates currents that map to the ionosphere and correspond to the NBZ currents.

The convection in the outer magnetosphere forms a pair of closed cells. Because particles can be trapped in this region for a long time, the plasma exhibits the characteristics of a steadily trapped population. The ionospheric footprint of this region is in the region equatorward of the polar caps. Any precipitation in this region should show magnetospheric type plasma. The convection in the outer magnetosphere is not directly driven in the magnetosphere because in ideal MHD there is no momentum transfer across streamlines. It is driven in the ionosphere by Pedersen currents. These Petersen currents are associated with the equatorward currents produced by the NBZ currents when they flow into and out of the ionosphere. In the ionosphere these currents can go under through the topological boundary between the outer magnetosphere and the LLBL/tail, because in the ionosphere the governing processes are not ideal MHD. Here we recall that the field-aligned current condition is derived from ideal MHD for low-β slowly-moving plasmas. The currents do not flow across the magnetic field lines or streamlines except in the equatorial region, where the β or velocity is not low and the currents are generated, and in the ionosphere, where ideal MHD needs to be replaced by non-ideal MHD. The Lorentz force (more accurately the electric field drift in the simulation) associated with these currents drives the ionospheric convection, and consequently maps to and drives the convection in the outer magnetosphere. For more detailed discussion of this coupling process, one is referred to *Song et al.*[1999].

In the following, we will provide more details of the solar wind-magnetosphere interaction portion of this global physical picture. The details of the ionosphere-magnetosphere coupling will be discussed in a later paper.

4. Results: In-depth Analysis

4.1. Bow Shock and Magnetopause Position

In the reference run, the bow shock is located at 14.3 R_E in the subsolar region, 23 R_E at the noon-midnight terminators, and 26.3 R_E at the equatorial terminators. If one fits the dayside bow shock with an ellipse, the eccentricity is 0.84 in the equatorial plane and 0.61 in the noon-midnight meridian plane. The simulation results are in general agreement with observations. The average observed eccentricity in the equatorial plane is 0.81 [*Farris et al.*, 1991].

In the reference run the last closed magnetic field line is located at 10.7 R_E in the subsolar region, 14.8 R_E at the noon-midnight terminators and 15.0 R_E at the equatorial terminators, indicating that the dayside magnetosphere is slightly elongated in the dawn-dusk direction. The empirical magnetopause location using the given values of B_z and solar wind dynamic pressure is 11.1 R_E at the subsolar point and 15.5 R_E at the equatorial terminator [*Shue et al.*, 1998]. The difference is within the resolution of the simulation and the uncertainty of the observations. It is worth mentioning that the subsolar magnetopause is defined in our case by the last closed magnetic field line, namely, point A in Plates 3a and 3b. If one follows the streamline along the Sun-Earth line, it splits at point B in Plate 3b, which is the inner edge of the LLBL, instead of the magnetopause.

Reconnection between the IMF and the magnetospheric field takes place at (1.6, 0, 13.2) R_E in the noon-midnight meridian, a few R_E tailward of the cusps. The magnetotail is 56 R_E long. Table 1 shows the results for different upstream conditions. The $B_z = 10$ nT run keeps all other parameters the same as the reference run but doubles the IMF strength. Similarly, the $n = 10$ cm^{-3} run only doubles the solar wind density.

The difference in the standoff distance between the 10 nT run and the reference run is smaller than a fraction of a grid size. At the same time the magnetopause becomes less flared. Such dependence is consistent with observations [*Shue et al.*, 1998]. The bow shock moves outward substantially and becomes more open, indicating a thicker magnetosheath for stronger IMF. As we know, the thickness of the magnetosheath is inversely proportional to the upstream magnetosonic Mach number. The higher IMF strength leads to a higher Alfvén velocity, and consequently, to a lower magnetosonic Mach number. The decreased magnetosonic Mach number results in a thicker magnetosheath. The increased IMF strength also results in a shorter magnetotail. This effect will be discussed later in the paper.

When the solar wind density is higher, the higher dynamic

Table 1. Locations of the Bow Shock, Magnetopause and Last Closed Field Line

Upstream	Bow Shock, R_E			Magnetopause, R_E			Tail, R_E
Condition	X	Y	Z	X	Y	Z	X
Reference	14.3	26.3	23	10.7(11.1)*	15.0(15.5)*	14.8	-56
10 nT	15.3	29.0	25	10.5	14.1	13.5	-32
10 cm^{-3}	12.2	22.5	21.9	9.4	15.0	13.7	-76.2

* Values in parentheses are from empirical model [*Shue et al.*, 1998].

pressure pushes the magnetopause inward by ~12%. An empirical scaling law of 1/6.6 [*Shue et al.*, 1998] translates a factor of 2 increase in the dynamic pressure into an 11% increase in the stand-off distance. This difference in the dependence of the subsolar magnetopause on the solar wind density between the simulation and the empirical model is below the resolution of the simulation, indicating that the model describes very well the stand-off distance of the magnetopause as well as its dependence on the solar wind dynamic pressure. The dawn-dusk terminator distance remains the same as the reference run, while the subsolar magnetopause is pushed inward, indicating that the magnetopause becomes more flaring. This tendency is also consistent with the empirical models [e.g., *Shue et al.*, 1998]. The higher solar wind density increases the magnetosonic Mach number via the Alfvén velocity, resulting in a thinner magnetosheath. This dependence is consistent with the simulation results. The magnetotail appears to be longer for the high-density run. This dependence will be discussed in more detail in section 4.4.

4.2. Magnetopause/Topological Boundary

Plate 4 shows the Y component of the electric currents in the noon-midnight meridian plane. On the dayside, most of the currents are generated at the bow shock. The Lorentz force due to these currents decelerates the solar wind flow. Most of the magnetopause current appears in the region upstream of the first closed magnetospheric field line. The observations of the sheath transition layer, or plasma depletion layer, are consistent with this region of current. The topological boundary itself contains little current and marks the inner edge of the magnetopause current. Observations have shown that for northward IMF the topological change occurs at the inner edge of the sheath transition layer [*Song et al.*, 1993].

On the nightside, the magnetopause current and the topological boundary of the magnetosphere become completely different. In the noon-midnight meridian plane most of the current is associated with magnetic field kinks located around 20 to 30 R_E above and below the equator, a region few satellites have visited yet. If one uses this current to define the boundary of the magnetosphere, the "magnetosphere" would appear to be open. Between the last closed field lines and the magnetopause current the magnetic field and particle characteristics are similar to (and observationally difficult to distinguish from) those in the closed magnetic field line region in the magnetotail. This is quite natural, since these field lines have just recently lost their topological connection with Earth. It will take an Alfvén traveling time for the field lines to communicate to the equatorial region of the flux tube about the fact that the magnetic field line has been disconnected at the cusp. It will take even longer before the plasma on these flux tubes can be assimilated to the solar wind. We should point out that the last closed field line on the nightside in Plate 3a corresponds to point a in Plate 3b, which is earthward of the shaded area. If one defines the magnetospheric topological boundary as the last closed field line, he/she may find a ditch on the nightside topological surface. This corresponds to the magnetic flux tube that has just been disconnected from the magnetospheric field. The size of the ditch is determined by the reconnection rate among other factors. In the equatorial plane, the magnetosphere may appear to have a pair of wings.

Near the cusps, there is a gap between the dayside current and nightside current. In a steady state, the dayside current is farther from the Earth than the nightside current. Some of these features can be better seen in the bottom-right panel of Plate 5. Therefore, for satellites flying through the cusp regions, multiple currents may be observed in a single pass for strongly northward IMF. The two currents are in the opposite direction, but the nightside branch has a stronger intensity in a larger region. We believe that part of the nightside current is closed via the bow shock current.

4.3. Formation of Low-Latitude Boundary Layer

The mechanisms leading to the formation of LLBL have always been an important subject for global magnetosphere models. The two major issues are (1) how particles enter the LLBL, and (2) what forces drive the flow. Previously proposed entry mechanisms include diffusion, reconnection and impulsive penetration. Since here we discuss only steady state solutions, impulsive penetration will not be considered.

We investigate the possibility of diffusive entry by tracing the plasma flux in the LLBL. In an MHD treatment, the diffusion broadens the region of density gradient. This causes real mass transfer if the topological boundary is located at the edge of the high-density region. In contrast, the diffusion in particle treatments can be different. The populations on the two sides of the boundary are different. Each of these populations diffuses according to the density gradient of their own population. Therefore the diffusion can be bidirectional. After particles are diffused across the boundary, their gyromotion and drift motion will spread these particles in the region away from the diffusion region. This results in a real particle flux transfer. From our MHD simulation results, we trace the magnetic field lines and determine the topological boundary in the equatorial plane. Plasma entry corresponds to streamlines crossing the magnetopause topo-

logical boundary. Since diffusion occurs in the entire magnetopause, one would expect that there are streamlines across the magnetopause over a very large region. In contrast, reconnection entry occur in a limited location near local noon. Near the dayside magnetopause, our grid size is 1 R_E, and it is doubled in the nightside. A coarser grid will result in a greater numerical diffusion. As shown in Plate 6a, in the equatorial plane, in a large region the streamlines are parallel to the magnetopause topological boundary, and hence no significant diffusion is present.

The plasma entry in our simulations is facilitated by reconnection that takes place at high latitudes. The reconnection process cuts the magnetosheath flux tubes and connects them with the magnetospheric flux tubes. These newly formed flux tubes bring the solar wind plasma as a whole into the magnetosphere with the same processes as described by *Song and Russell* [1992] and *Song et al.* [1994]. Most of the particle entry is concentrated in the subsolar region. In contrast, the entry for the diffusion should occur relatively uniformally in a large spatial region.

In an MHD treatment, the forces acting on a flow can, in principle, be the viscous force, pressure gradient force and Lorentz force. In the LLBL, the Lorentz force associated with the currents created by the magnetic field distortion is sunward pointed and hence cannot be a driving force. We will evaluate the importance of the viscous force in section 4.4 when we discuss the length of the tail. It will show that the viscous force has very limited effects on the flow.

As shown in Plate 1a, the pressure near the subsolar magnetopause is ~27 times higher than that near the last closed magnetic field line in the midnight. The pressure outside the last closed magnetic field line in the midnight is even lower, which provides an additional sucking force. This lower-pressure region is associated with the change in the direction of the magnetic curvature force. With the large pressure gradient, the magnetosheath plasma entered in local noon experiences an expansion while being dragged at their feet in the ionosphere as described by *Song and Russell* [1992], *Yang et al.* [1994], and *Song et al.* [1994]. Further evidence for the pressure driven can be found in Plate 6b. The streamlines in the distant tail region are nearly perpendicular to the contours of the pressure. Namely, the flow is moving antiparallel to the pressure gradient. Therefore we conclude that the LLBL is primarily driven by the pressure gradient force. In a highly simplified model, *Song et al.*, [1994] neglected the gradients normal to the boundary layer. Our simulation has shown that gradients do exist normal to the boundary and can be large in the flanks and nightside; see Plate 6a for example. Therefore, the observations of the density gradient and velocity shear [*Phan et al.*, 1997] may not be necessarily caused by viscous or diffusive processes.

4.4. Length of the Tail

Because the length of the tail is one of few characteristic parameters that specify the size of the magnetosphere, it has attracted continuous interest. To us, the most critical issue is to understand the dependence of the tail length on various upstream parameters and hence the physical processes involved. As seen in Plate 3b, in a closed magnetosphere model, the length of the magnetotail is determined by the processes that drive and impede the LLBL flow.

We first examine the effects of the viscous interaction. In our numerical model, there is no physical viscosity. The viscosity arises owing to the numerical discretization. The numerical viscosity is proportional to the size of a simulation cell. A lower spatial resolution in the simulation results in a higher numerical viscosity. As shown in Plate 5, we have made several runs with different spatial resolutions while keeping other parameters the same [*Gombosi et al.*, 1998]. The resolution is inversely proportional to the number of cells in each run as labeled above each panel. The color coding represents the intensity of the currents. As the resolution increases, one can see better resolved currents. For the lowest resolution run, the tail is 58 R_E long. As the resolution increases, the tail shortens to 55 R_E. (Here we should point out that the length of the tail for the runs using the same upstream parameters as the reference run may be slightly different because it is obtained from different setting. However, each of the runs is compared with other runs under the same setting.) The tail length remains essentially unchanged as the resolution becomes higher and higher. Therefore one may conclude that the tail in our high-resolution runs is not driven significantly by the viscous force.

As discussed in the last section and shown in Plates 5 and 6b, the driving force for the LLBL/tail is the pressure gradient force from the dayside to the nightside and the drag force is the Lorentz force associated with the cross-tail current. Most of the cross-tail current is closed with the nightside "magnetopause" current, and a small portion eventually is diverted to become the field-aligned currents, maps to the ionosphere, and dissipates there [*Sonnerup*, 1980a]. The length of the tail is determined by the balance between the driving and drag forces [*Song et al.*, 1999].

As pointed out by *Song and Russell* [1992], the driving pressure is proportional to $\sqrt{1+\beta}+1$, where β is the magnetosheath plasma beta near the magnetopause topological boundary at local noon. In the distant tail, the magnetic field is highly stretched and the Lorentz force there may only be a weak function of distance. The magnetosheath "plasma parameter" $\sqrt{1+\beta}+1$ near the subsolar magnetopause becomes the key parameter determining the length of the tail. Figure 1a shows the dependence of the tail length on the magnetosheath plasma parameter. There is a general linear relationship between the two. In these runs, the solar wind velocity and temperature, and the ionospheric conductivity are the common parameters. In addition to the solar wind density and the IMF strength, the spatial resolution and the grid distribution are not the same because the results are collected from runs for different purposes. The differences in the grid distribution and in spatial resolution will cause scattering in the comparison. The linear relationship indicates that the pressure gradient forces (not the pressure itself) in

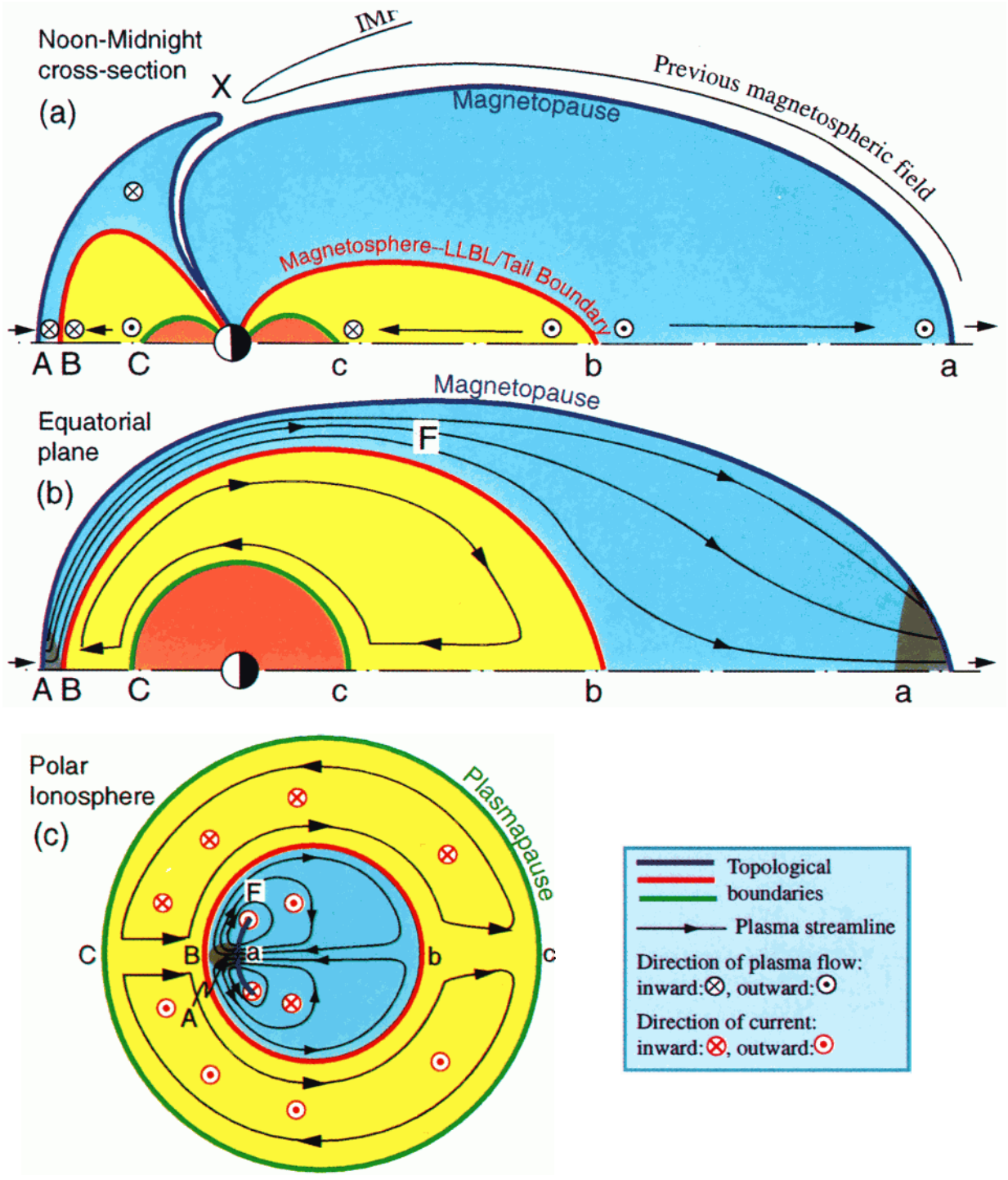

Plate 3. Global geometry of the magnetosphere and ionospheric mapping [*Song et al.*, 1999]. In all panels, thick solid lines represent the separatrix surfaces and thin solid lines with arrowheads indicate the direction of the flow, and the shaded areas indicate the regions ambient to newly reconnected/disconnected magnetic field lines the topological status of which is ambiguous. (a) The noon-midnight meridian plane of the magnetosphere viewed from dusk. Circles with crosses (dots) indicate the plasma flows away from (toward) the reader on the morning side, but is diverted before reaching the noon-midnight meridian plane. The magnetopause/cusp is the surface consisting of curves A-X-Earth on the dayside and Earth-a on the nightside. The boundary between the outer magnetosphere and LLBL/tail consists of curves B-Earth on the dayside and Earth-b on the nightside, and the plasmapause consists of curves C-Earth and Earth-c. (b) The equatorial plane of the magnetosphere viewed from north. Point F indicates where the boundary layer streamline turns from away from sun-Earth line to toward the sun-Earth line, and maps to the ends of the cusp arc in Plate 3c. (c) The northern ionosphere viewed from top. The circles with dots and crosses indicate the directions of the field-aligned currents, instead of the plasma flows.

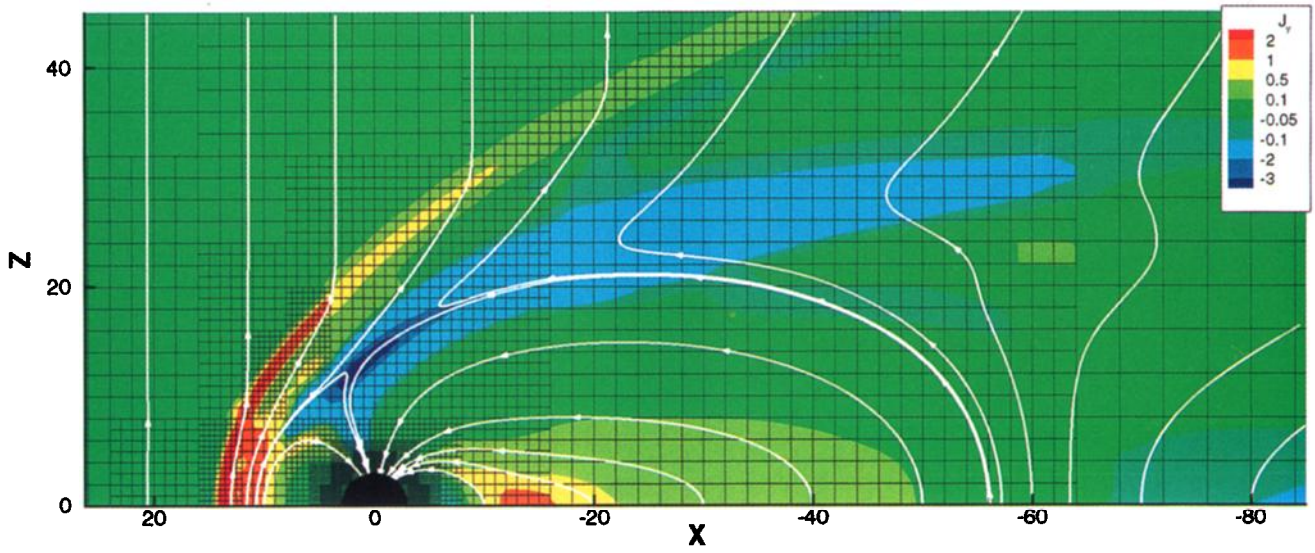

Plate 4. The currents in the noon-midnight meridian plane. The color coding shows the Y component of the current density.

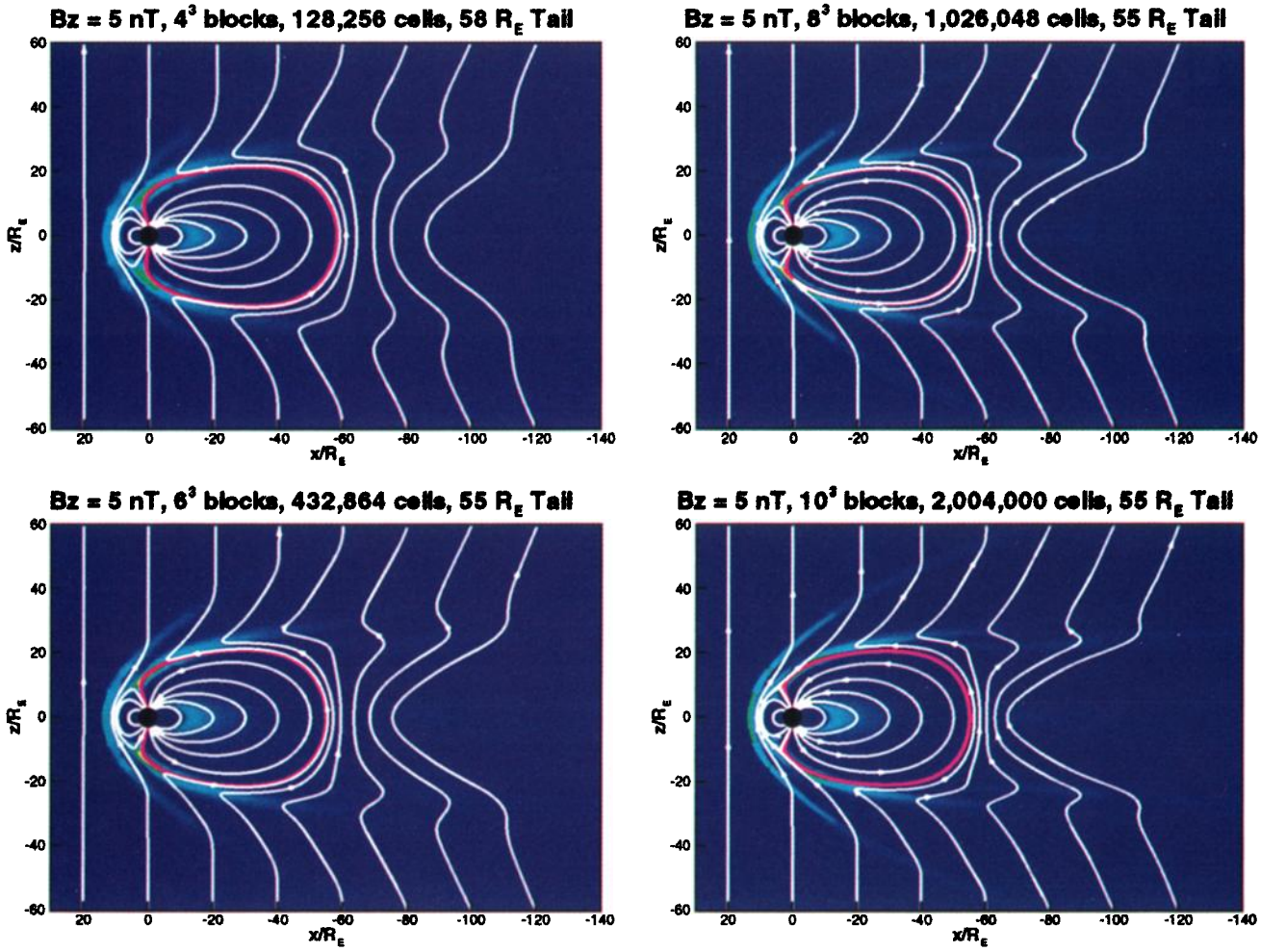

Plate 5. The length of the tail with different spatial resolutions [*Gombosi et al.*, 1998]. The resolution is proportional to the cubic root of the number of cells which is indicated above each frame. The color coding indicates the magnitude of the electric currents. The last closed magnetic field line is indicated by the purple line in each frame.

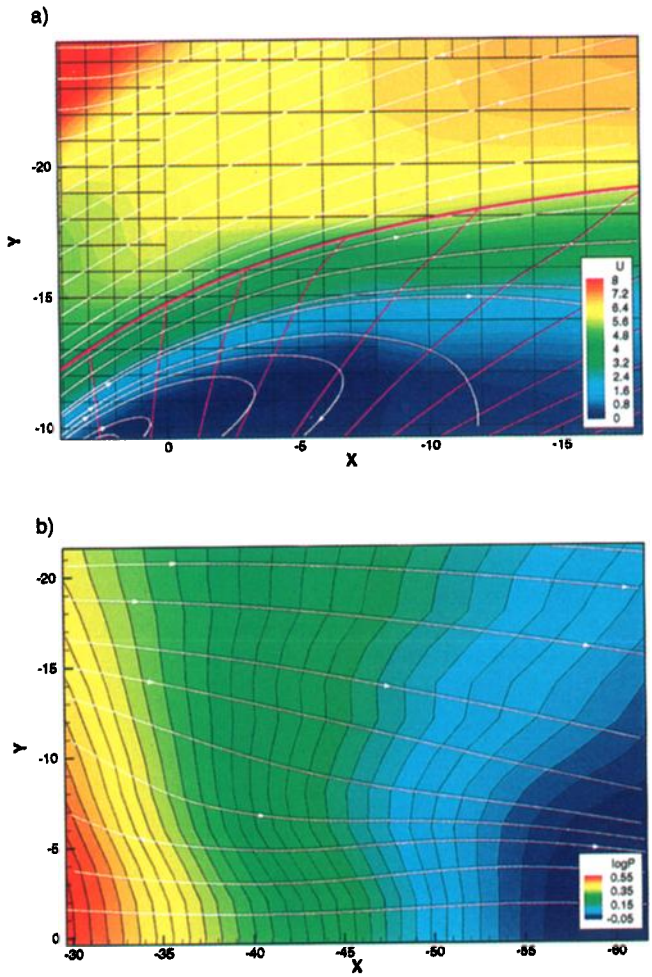

Plate 6. (a) Zoom-in of the flank LLBL region in the equatorial plane. The thin pink lines are projection of the last closed magnetic field lines onto the equatorial plane. The thick pink line indicates the locus of the last closed magnetic field lines. The color coding shows the velocity normalized by the solar wind sound speed and the white lines with arrowheads are plasma streamlines. (b) Zoom-in of the distant tail equatorial region. The color coding shows the logarithm of the thermal pressure and the black lines are pressure contours. The white lines with arrowheads are streamlines.

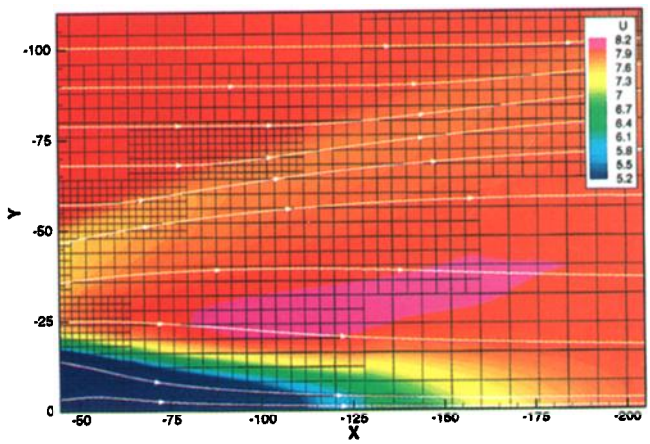

Plate 7. Velocity distribution in the equatorial plane. The color coding shows the velocity normalized by the solar wind sound speed, which is 50 km/s, and the white lines with arrowheads are plasma streamlines. The region of high-speed flow above the solar wind with Mach number 8 is highlighted in purple.

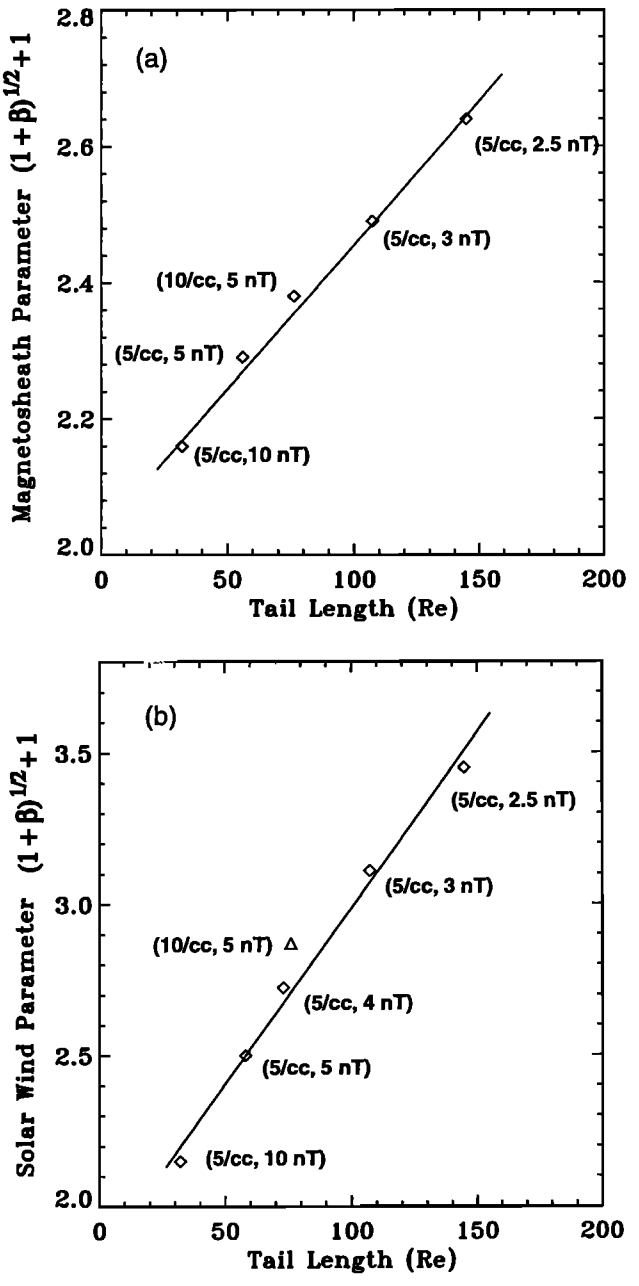

Figure 1. (a) Dependence of the tail length on the magnetosheath plasma parameter $\sqrt{1+\beta}+1$. (b) Dependence of the tail length on the solar wind plasma parameter $\sqrt{1+\beta}+1$. The 4 nT case in Figure 1b was archived graphically but not digitally. The magnetosheath plasma parameter for this case is not available.

different runs remain similar. A higher initial pressure simply stretches the tail longer. This is consistent with our understanding that the tail length is determined by the balance between the driving and drag forces. Here we should point out that because the field-aligned currents are derived from only a small portion of the tail currents, the ionospheric drag may have only very limited effects on determination of the length of the tail. The conclusion we draw from this analysis is that our numerical model is consistent with the theoretical model in which the LLBL is primarily driven by the pressure gradient force associated with cusp reconnection entry processes. If there were a significant viscous force, one would expect the curve to become flat at larger values of the tail length. As shown in Figure 1a, up to 150 R_E, the effect of the viscous force is not very strong.

Gombosi et al. [1998] reported that the tail length is approximately proportional to the reciprocal of the strength of the IMF. Figure 1b shows the results of the tail length as functions of the solar wind plasma parameter from simulations. It is clear that when the solar wind density remains the same, the tail length depends linearly on the solar wind plasma parameter. When the solar wind density changes, because of the processes at the bow shock and in the magnetosheath, the plasma parameter near the magnetopause changes at a slightly different rate from the trend by varying the magnetic field strength.

We now examine the effects of the solar wind Mach number. Since the tail length is proportional to the magnetosheath plasma beta near the subsolar magnetopause, it is proportional to the plasma beta downstream of the bow shock. To understand what determines the plasma beta downstream of the bow shock, we first take a look at the change in the length of a magnetic field line, which equals the ratio of the magnetic field strength and plasma density. When the IMF is tangent to the subsolar bow shock, there is little stretching or shortening in the magnetic field lines across the bow shock. The length of a magnetic field line remains similar across the bow shock. The plasma beta downstream of the bow shock will then be proportional to the ratio of the plasma heating factor, which determines the downstream temperature, to the magnetic field compression factor. In the range of normal solar wind Mach number, the heating factor increases with the Mach number much faster than the magnetic field compression factor does. For a higher sonic Mach number, the magnetosheath β will be higher leading to a longer tail. This is confirmed by a pair of runs with a sonic speed of 40 km/s and sonic Mach numbers 10 and 8, respectively. The tail is 58 R_E long for the Mach 10 run and 51 R_E for the Mach 8 run. Unfortunately, the plasma parameters near the subsolar magnetopause for these two cases were not documented.

The effect of the sonic speed or solar wind temperature alone is more complicated. A high sonic speed will reduce the solar wind Mach number and hence the heating at the bow shock. However, depending on whether the reduction of the heating can make up the higher upstream temperature, the resulting temperature downstream of the bow shock may be either higher or lower or same. Therefore the tail may be either longer or shorter or same depending on the value of the Mach number.

5. Discussion

5.1. Definition of the Magnetopause

The definition of the magnetopause was once thought simple and straightforward. However, it is not trivial for northward IMF. Using the conventional definition of the magne-

topause, the region containing most of the current, the magnetopause identified using the magnetometer [*Russell and Elphic*, 1978], which is most sensitive to the currents, is the plasma depletion layer identified using the particle measurements [*Paschmann et al.*, 1978], which are most sensitive to particle characteristics but not the currents. After investigating this inconsistency, *Song et al.* [1993] suggested that the magnetopause should be defined as a physical concept instead of a single signature measured by a particular instrument. A particular signature measured by a certain instrument should be used to determine the relative location of the satellite within the overall structure. The physical meaning of the signature may change with the IMF conditions. Our simulations show clearly the difference between the topological boundary and the magnetopause current in the subsolar region. In the cusp regions, their relationship becomes even more complicated.

To define of the magnetopause in the distant tail is more difficult as the topological boundary becomes irrelevant to the current. One may suggest to define the magnetopause according to the topological boundary. However, according to the standard pictures, the magnetotail neutral sheet current is closed with the magnetopause current in the distant tail. The topological boundary cannot provide the current closure. When one draws a θ-type tail current system, he/she includes topologically magnetosheath region in the magnetotail.

It is an observational challenge to identify the last closed magnetic field line in the distant tail near the equatorial plane. Immediately downstream of the last closed magnetic field line, both the magnetic field and plasma are indistinguishable from the magnetospheric ones. It moves slower than the solar wind, as shown in Plate 7, and almost empty with the solar wind population. The magnetic field would be dominated by the Z component. The X component will reverse its polarity further downsteam. For the reference run, it will go up to 200 R_E downstream from the Earth before the flow becomes similar to the solar wind speed, as shown in Plate 7. The plasma density and pressure will remain significantly smaller than the solar wind values event after 250 R_E. For the 10 nT run, the flow velocity reaches the sheath speed at $\sim$50 R_E and reaches the solar wind speed at $\sim$75 R_E. After 50 R_E, the density and pressure starts increasing, but it is not able to reach the solar wind density within 250 R_E. Nevertheless, observations of absence of the magnetotail 200 R_E downstream from the Earth have been reported a few times [*Fairfield*, 1993; *Fairfield et al.*, 1996], supporting closed magnetosphere models.

Although the magnetopause topological boundary separates the solar wind from the magnetosphere domain, it is not a tangential discontinuity in local noon and midnight where solar wind fluxes enter and tail fluxes exit the magnetospheric domain. To understand the steady state processes of the solar wind entry, one can follow the motion of magnetic field lines in Plate 3a starting at the cusp based on the Petschek reconnection picture [*Petschek*, 1964]. He/she can see that the magnetic field line near point A moves Earthward. The magnetic field line then moves into or out of the page before it reaches point B. It is worth mentioning that the stagnation point is point B and not point A in Plates 3a and 3b, although the flow velocity drops significantly across the magnetopause topological boundary. Because point A is not a stagnation point, the mathematical singularity discussed by *Sonnerup* [1980b] does not exist at the magnetopause. Because the topological change occurs at point A, the magnetic field is magnetospheric at point B. The flux tube splits at local noon and the plasma flows azimuthally to the morning or evening side. This is consistent with the idea of the stagnation line proposed by *Sonnerup* [1980b] to solve the dilemma. Therefore the long-standing problem of stagnation point versus stagnation line is solved.

5.2. Cusp Reconnection

Reconnection on the nightside of the cusps for northward IMF was first proposed by *Dungey* [1961]. *Song and Russell* [1992] summarized indirect evidence for such a process. *Gosling et al.*, [1991], *Feldman et al.* [1995] and *Kessel et al.* [1996] provided more direct evidence. In particular, *Feldman et al.* [1995] showed evidence for conjugate reconnection in the two hemispheres. Similar evidence was also shown in laboratory simulations of the magnetosphere [*Dubinin and Potamu*, 1981]. Cusp reconnection has been shown in all computer simulation models for northward IMF as we summarized in the introduction section.

There has been debate over whether the reconnection process at the two cusps takes place simultaneously on the same flux tube. Our simulation domain and IMF conditions are symmetric with respect to the XY and XZ planes. No appreciable difference is found between the two hemispheres in our simulations. Therefore, in principle, the reconnection process at the two cusps takes place simultaneously on the same magnetic field line. Here we caution against simple use of the magnetic field line tracing program to identify whether the reconnection process is symmetric. Because the magnetic field near the reconnection site is very weak, the uncertainty in the magnetic field line tracing is large. If one uses a symmetric simulation setup and concludes that the reconnection process is not symmetric, a physical explanation is needed.

When the IMF has an X component or the geomagnetic dipole is tilted in the X direction, the north-south symmetry will break. It is possible that the reconnection process at the two cusps is not simultaneously on the same flux tube. Each hemisphere may develop an open magnetic field line region. If the reconnection rates are same at the two cusps, the trailing reconnection event has no direct effect on the ionospheric convection pattern and topological boundaries in the hemisphere corresponding to the leading reconnection event. This is because the electric field associated with the first reconnection event will map along the magnetic field line to the other hemisphere. It equals the electric field associated with the second reconnection event. The second reconnection event does not send an additional electric field to the other foot of the flux tube.

5.3. Cusp and Polar Cap

In a static closed magnetosphere model which assumes the magnetosphere to be vacuum without convection, the last closed magnetic field lines converge along the magnetopause to a singular point at each cusp and then map to the ionosphere at the magnetic pole in each hemisphere [e.g., *Crooker*, 1979; *Siscoe*, 1988]. When convection is added to such a model, the electric field near the poles becomes singular and hence the model cannot be completely self-consistent. Various ad hoc ways have been thought to remove the singular points [e.g., *Siscoe*, 1988; *Toffoletto and Hill*, 1989]. In our model, the magnetosphere is not empty and it is in motion. The magnetospheric motion is coupled to the ionosphere via the line-tie process [*Coroniti and Kennel*, 1973]. For the magnetic field lines near the magnetopause, when they convect from the dayside to the nightside, their ionospheric footprints convect with them. Therefore the magnetopause maps to an extended line in local time in the ionosphere as shown in Plate 3c, rather than a singular point, in each hemisphere. The dayside and nightside branches of the magnetopause map back-to-back in the ionosphere separated by the topological boundary, which can be interpreted as the ionospheric cusp. However, the physical solutions at this line of topological boundary are not singular but discontinuous when mapping to the high-altitude magnetosphere.

The polar cap referred to in our discussion is a high-latitude ionospheric region which has different observational characteristics from the midlatitude ionosphere. Our definition may be different from that used in ionospheric observations. According to our definition and our model, this region should observe low-energy precipitation particles of solar wind origin because it corresponds to the LLBL/tail region in the magnetosphere. The fresh solar wind flux will have the highest intensity near the cusp which is located at $\sim 83°$ latitude with some spread around the local noon, because in the cusp region, the solar wind can have a large field-aligned population. As the flux tubes move tailward in the LLBL, they continuously lose the field-aligned component of the particles. The pitch angle diffusion due to the wave-particle interaction will provide field-aligned particles but at a lower flux. Therefore we expect that the precipitation will be significantly lower on the nightside of the cusps than in the dayside cusps. In contrast, low latitudes to the polar cap map to the outer magnetosphere where there is little solar wind population. We expect that the ionospheric precipitation is dominated by particles of magnetospheric origin. The flux should be lower, and the energy should be higher.

In ionospheric observations, the polar cap is often referred to as the region without particle precipitation of solar wind origin. This definition of the polar cap is based on the physical processes for southward IMF. Observations have shown that such defined polar cap may be absent for northward IMF [*Newell et al.*, 1997]. Instead, during these periods the ionospheric DMSP satellites observed low-energy precipitation. These observations are consistent with our model expectations. We note that ionospheric observations have been interpreted to indicate a closed magnetosphere for northward IMF [*Troshichev and Nishida*, 1992; *Newell et al.*, 1997]. *Newell et al.* [1997] further pointed out that a short interval of southward IMF fluctuations can lead to a much longer duration of ionospheric signatures that are associated with an open magnetosphere. Ionospheric signatures for quasi-steady state northward IMF may be more difficult to identify and are certainly rare.

5.4. Effects of Ionospheric Boundary Conditions

As the first step to model the magnetosphere–ionosphere interaction, we have used a highly simplified ionospheric model. The Petersen conductance has been assumed to be uniform and stationary. In reality, the conductance depends on local time and latitude, and varies with magnetospheric precipitations. The following discussion is based on our understanding of the formulisms employed in our model and does not necessarily describe the processes taking place in reality. The effects will be investigated and reported in our future papers.

As seen from equation (5), the spatial variation of the conductance can be considered as a source, in addition to the field-aligned currents, of the divergence of the electric field, and hence the rotation of the velocity field. If the centers of the field-aligned currents are associated with a higher conductance (which may not be always true), the effect of the conductance gradients tends to enhance the convection driven by the Petersen currents. If the total amount of the field-aligned current, which may be determined by the magnetic field distortion, in particular by magnetic field shears, is fixed for a given solar wind condition, the effect of the conductance gradients may be an enhanced ionospheric convection. Consequently, the enhanced ionospheric convection will be coupled to the magnetosphere. It would be interesting to see, in our future simulations, whether the enhanced magnetospheric convection would lead to a longer magnetotail or not, because this process, as is described, is a positive feedback process. Nevertheless, when including the gradients in the conductances, we expect that the conclusions drawn in our study remain qualitatively valid.

In this study, we have not included the Hall currents. In a steady state, the electric field is curl-free. Combining this condition with the uniform conductance condition used in the simulation, the Hall conductance will have no effect on the magnetosphere-ionosphere coupling described by equation (5) evenif we had assumed the Hall conductance to have a finite value. The effects of the Hall currents will appear when allowing gradients in the conductances. These effects remain to be investigated.

As discussed in section 4.4, because the ionospheric drag contributes to only a small fraction of the total magnetotail drag, we expect that the ionospheric conductance will have only minimal effects on the tail length.

5.5. High Speed Sheath Flow

Chen et al. [1993] reported the observations of the magnetosheath flow that moves faster than the solar wind speed. In our reference simulation run, a fast flow does occur in the equatorial plane, but it starts at $\sim 75\ R_E$ tailward of the Earth, as shown in Plate 7, and centered around 100 R_E.

This region can be as close as 20 R_E and centered at 50 R_E for the 10 nT case. The maximum magnitude of the speed is less than 5% higher than the solar wind speed for the reference run and slightly more than 10% for the 10 nT case. In the noon-midnight meridian plane, similar fast flow also exists. Nevertheless, the outward motion of the subsolar magnetopause with increasing positive B_z inferred by *Chen et al.* [1993] is not shown in our simulations, as shown in Table 1.

6. Conclusions

We have simulated the solar wind-magnetosphere-ionosphere system for due northward IMF using several different upstream parameters and spatial resolutions. Qualitatively, there is a steady state solution for the system. This solution is independent of the initial conditions. This steady state solution can be understood physically. Changes in the upstream conditions and spatial resolutions result in quantitative differences in the solution. We have not seen drastic fundamental changes in response. We conclude that the system has at least one steady state solution although we cannot exclude the possible existence of other steady state solutions. No critical stage in the reasonable range of upstream conditions has been observed.

In this steady state solution, the magnetosphere is essentially closed except for two small regions near the cusps where reconnection between the IMF and magnetospheric field takes place. There are three topologically separated regions. The LLBL/tail region is directly driven by the reconnection process. Mapping to the ionosphere, this region corresponds to the polar cap region, sunward convection cells and NBZ currents. The outer magnetosphere is topologically insulated from the solar wind driver. It forms a pair of convection cells and maps to the ionospheric antisunward convection cells and region I currents. The driver of the magnetospheric convection cells is the ionospheric Pedersen currents resulted from the diversion of the NBZ currents. The Pedersen currents couple energy across the topological boundary between the LLBL and outer magnetosphere and generate the convection electric field. Since the physical processes in the inner magnetosphere are not adequately described in our model, we do not discuss the inner magnetosphere region.

Our simulations indicate that the LLBL plasma is primarily provided by reconnection. Diffusion may play only a minor role in causing the particle entry. The LLBL convection is primarily driven by the pressure force although the viscous force may contribute slightly to driving the LLBL flow.

The length of the magnetotail has a linear relationship with the magnetosheath plasma parameter $\sqrt{1+\beta}+1$. The higher the subsolar magnetosheath plasma parameter is, the longer the tail. For a fixed solar wind density, velocity, and temperature, the subsolar magnetosheath plasma parameter is proportional to the solar wind plasma parameter. Since the plasma parameter describes the driving force of the LLBL flow, we conclude that the length of the magnetotail is determined primarily by the LLBL driving force.

The simulation results also raise a few issues as how to interpret observations. Topological boundaries seen in simulations are of global nature. The local plasma and magnetic field diagnostics may not be always directly related to the changes in global topology. One example is the last closed magnetic field line on the nightside. It is observationally challenging to identify the last closed magnetic field line. The topological boundary between the magnetosheath and the magnetosphere is located at the inner edge of the magnetopause current layer in the subsolar region and has little relevance to the magnetopause current in the distant tail. Likewise, the signatures and definition of the polar cap need to be reviewed according to IMF conditions.

Acknowledgments. This work was supported by NSF/ONR under Award NSF-ATM9713492, by the NSF-NASA-AFOSR interagency grant NSF ATM-9318181, and by NASA HPCC Grand Challenge Cooperative Agreement NCCS5-146.

Janet G. Luhmann thanks Michael Goodman and Olaf Amm for their assistance in evaluating this paper.

References

Amm, O., Comment on "A three-dimensional, iterative, mapping procedure for the implemenation of an ionosphere-magnetosphere anisotropic Ohm's law boundary condition in global magnetohydrodynamic simulations" by Michael L. Goodman, *Ann. Geophys.*, *14*, 773, 1996.

Angelopoulos, V., et al., Statistical characteristics of bursty bulk flow events, *J. Geophys. Res.*, *99*, 21,257, 1994.

Berchem, J., J. Raeder, and M. Ashour-Abdalla, Reconnection at the magnetospheric boundary: Results from global magnetohydrodynamic simulations, in *Physics of the Magnetopause, Geophys. Monogr. Ser.*, vol. 90, edited by P. Song, B. Sonnerup, and M. Thomsen, p. 205, AGU, Washington, D. C., 1995.

Burch, J. L., N. A. Saflekos, D. A. Gurnett, J. D. Craven, and L. A. Frank, The quiet time polar cap: DE 1 observations and conceptual model, *J. Geophys. Res.*, *97*, 19,403, 1992.

Burke, W. J., M. C. Kelley, R. C. Sagalyn, M. Smiddy, and S. T. Lai, Polar cap electric field structures with a northward interplanetary magnetic field, *Geophys. Res. Lett.*, *6*, 21, 1979.

Chen, S., M. G. Kivelson, J. T. Gosling, R. J. Walker, and A. J. Lazaru, Anomalous aspects of magnetosheath flow and of the shape and oscillations of the magnetopause during an interval of strongly northward interplanetary magnetic field, *J. Geophys. Res.*, *98*, 5727, 1993.

Clauer, C. R., and E. Friis-Christensen, High latitude dayside electric fields and currents during strong northward IMF: Observations and model simulation, *J. Geophys. Res.*, *93*, 2749, 1988.

Coroniti, F. V., and C. F. Kennel, Can the ionosphere regulate magnetospheric convection?, *J. Geophys. Res.*, *78*, 2837, 1973.

Crooker, N. U., Dayside merging and cusp geometry, *J. Geophys. Res.*, *84*, 591, 1979.

Crooker, N. U., Reverse convection, *J. Geophys. Res.*, *97*, 19,363, 1992.

Dubinin, E., and Y. Potamu, The phenomena at the magnetospheric boundary and the convection in the polar cap, *Cosmic Res.*, *19*, 409, 1981.

Dungey, J. W., Interplanetary magnetic field and the auroral zones, *Phys. Rev. Lett.*, *6*, 47, 1961.

Fairfield, D. H., Solar wind control of the distant magnetotail: ISEE 3, *J. Geophys. Res.*, *98*, 21,265, 1993.

Fairfield, D. H., R. P. Lepping, L. A. Frank, K. L. Ackerson, W. R. Paterson, S. Kokubun, T. Tamamoto, K. Tsuruda, and M. Nakamura, Geotail observations of an unusual magnetotail under very northward IMF conditions, *J. Geomagn. Geoelectr.*, *48*, 473, 1996.

Farris, H., S. M. Petrinec, and C. T. Russell, The thickness of the magnetosheath: Constraints on the polytropic index, *Geophys. Res. Lett.*, *18*, 1821, 1991.

Fedder, J. A., and J. G. Lyon, The Earth's magnetosphere is 165 R_e long: Self-consistent currents, convection, magnetospheric structure, and processes for northward interplanetary magnetic field, *J. Geophys. Res.*, *100*, 3623, 1995.

Feldman, W. C., et al., Possible conjugate reconnection at the high-latitude magnetopause, *J. Geophys. Res.*, *100*, 14913, 1995.

Gombosi, T. I., D. L. DeZeeuw, R. M. Häberli, and K. G. Powell, Three-dimensional multiscale MHD model of cometary plasma environments, *J. Geophys. Res.*, *101*, 15,233, 1996.

Gombosi, T. I., D. L. DeZeeuw, C. P. T. Groth, K. G. Powell, and P. Song, The length of the magnetotail for northward IMF: Results of 3D MHD simulations, in *Physics of Space Plasmas (1998)*, edited by T. Chang, and J. R. Jasperse, vol. 15, p. 121, MIT Press, Cambridge, 1998.

Goodman, M. L., A three-dimensional, iterative, mapping procedure for the implemenation of an ionosphere-magnetosphere anisotropic Ohm's law boundary condition in global magneto-hydrodynamic simulations, *Ann. Geophys.*, *13*, 843, 1995.

Iijima, T., T. A. Potemra, L. J. Zanetti, and P. F. Bythrow, Large-scale Birkeland currents in the dayside polar region during strongly northward IMF: A new Birkeland current system, *J. Geophys. Res.*, *89*, 7441, 1984.

Jackson, J. D., *Classical Eelectrodynamics*, John Wiley, New York, 1975.

Kan, J. R., and W. J. Burke, A theoretical model of polar cap auroral arcs, *J. Geophys. Res.*, *90*, 4171, 1985.

Kessel, R. L., et al, Evidence of high-latitude reconnection during northward IMF: Hawkeye observations, *Geophys. Res. Lett.*, *23*, 583, 1996.

Linde, T. J., A three-dimensional adaptive multifluid MHD model of the heliosphere, Ph.D. thesis, Univ. of Mich., Ann Arbor, 1998.

Mobarry, C. M., J. A. Fedder, and J. G. Lyon, Equatorial plasma convection from global simulations of the Earth's magnetosphere, *J. Geophys. Res.*, *101*, 7859, 1996.

Newell, P. T., D. Xu, C. Meng, and M. G. Kivelson, Dynamic polar cap: A unified approach, *J. Geophys. Res.*, *102*, 127, 1997.

Ogino, T., and R. J. Walker, A magnetohydrodynamic simulation of the bifurcation of tail lobes during intervals with a northward interplanetary magnetic field, *Geophys. Res. Lett.*, *11*, 1018, 1984.

Paschmann, G., N. Sckopke, G. Haerendel, I. Papamastorakis, S. J. Bame, J. R. Asbridge, J. T. Gosling, E. W. Hones Jr., and E. R. Tech, ISEE plasma observations near the subsolar magnetopause, *Space Sci. Rev.*, *22*, 717, 1978.

Petschek, H. E., Magnetic field annihilation, in *AAS-NASA Symposium of the Physics of Solar Flares, NASA Spec. Publ., NASA-SP 15*, 1964.

Phan, T.D., et al., Low-latitude dusk flank magnetosheath, magnetopause, and boundary layer for low magnetic shear: Wind observations, *J. Geophys. Res.*, *102*, 19883, 1997.

Powell, K. G., An approximate Riemann solver for magnetohydrodynamics (that works in more than one dimension), *Tech. Rep. 94-24*, Inst. for Comput. Appl. in Sci. and Eng., Langley, Va, 1994.

Powell, K. G., P. L. Roe, R. S. Myong, T. I. Gombosi, and D. L. DeZeeuw, An upwind scheme for magnetohydrodynamics, in *Proceedings of AIAA 12th Computational Dynamics Conference*, no. AIAA-95-1704, p. 661, Am. Inst. of Aeronaut. and Astronaut. New York, 1995.

Powell, K. G., P. L. Roe, T. J. Linde, T. I. Gombosi, and D. L. DeZeeuw, A solution-adaptive upwind scheme for ideal magnetohydrodynamics, *J. Comput. Phys.*, in press, 1999.

Raeder, J., The effect of electrical resistivity on the topology of the magnetosphere, *Eos Trans. AGU*, 79(45), Fall AGU Meet., F746, 1998.

Raeder, J., R. J. Walker, and M. Ashour-Abdalla, The structure of the distant geomagnetic tail during long periods of northward IMF, *Geophys. Res. Lett.*, *22*, 349, 1995.

Reiff, P. H., and J. L. Burch, IMF b_y-dependent plasma flow and Birkeland currents in the dayside magnetosphere, 2, A global model for northward and southward IMF, *J. Geophys. Res.*, *90*, 1595, 1985.

Roe, P. L., Approximate Riemann solvers, parameter vectors, and difference schemes, *J. Comput. Phys.*, *43*, 357–372, 1981.

Russell, C. T., The configuration of the magnetosphere, in *Critical Problems of Magnetospheric Physics*, edited by E. R. Dyer, p. 1, Nat. Acad. of Sci., Washington, D. C., 1972.

Russell, C. T., and R. C. Elphic, Initial ISEE magnetometer results: Magnetopause observations, *Space Sci. Rev.*, *22*, 681, 1978.

Shue, J.-H, P. Song, C. T. Russell, J. T. Steinberg, J. K. Chao, G. Zastenker, O. L. Vaisberg, S. Kokubun, H. J. Singer, T. R. Detman, and H. Kawano, Magnetopause location under extreme solar wind conditions, *J. Geophys. Res.*, *103*, 17,691, 1998.

Siscoe, G. L., The magnetospheric boundary, in *Physics of Space Plasmas (1987)*, edited by T. Chang et al., p. 3, Sci. Publishers, Cambridge, Mass., 1988.

Song, P., C. T. Russell, D. J. Fitzenreiter, J. T. Gosling, M. F. Thomsen, D. G. Mitchell, S. A. Fuselier, G. K. Parks, R. R. Anderson, and D. Hubert, Structure and properties of the subsolar magnetopause for northward IMF: Multiple instrument particle observations, *J. Geophys. Res.*, *98*, 11,319, 1993.

Song, P., and C. T. Russell, A model of the formation of the low latitude boundary layer, *J. Geophys. Res.*, *97*, 1411, 1992.

Song, P., T. Holzer, C. T. Russell, and Z. Wang, Modeling the low latitude boundary layer with reconnection entry, *Geophys. Res. Lett.*, *21*, 625, 1994.

Song, P., T. I. Gombosi, D. L. DeZeeuw, and K. G. Powell, A model of solar wind-magnetosphere-ionosphere coupling for northward IMF, *Planet. Space Sci.*, in press, 1999.

Sonnerup, B. U. O., Theory of the low-latitude boundary layer, *J. Geophys. Res.*, *85*, 2017, 1980a.

Sonnerup, B. U. O., Transport mechanisms at the magnetopause, in *Dynamics of the Magnetosphere*, edited by S. -I. Akasofu, p. 77, D. Reidel, Hingham, Mass., 1980b.

Taguchi, S., and R. A. Hoffman, Control parameters for polar ionospheric convection patterns during northward interplanetary magnetic field, *Geophys. Res. Lett.*, *23*, 637, 1996.

Toffoletto, F. R., and T. W. Hill, Mapping of the solar wind electric field to the Earth's polar caps, *J. Geophys. Res.*, *94*, 329, 1989.

Troshichev, O. A., and A. Nishida, Pattern of electron and ion precipitation in northern and southern polar regions for northward interplanetary magnetic field conditions, *J. Geophys. Res.*, *97*, 8337, 1992.

Usadi, A., A. Kageyama, K. Watanabe, and T. Sato, A global simulation of the magnetosphere with a long tail: Southward and northward interplanetary magnetic field, *J. Geophys. Res.*, *98*, 7503, 1993.

Wu, C. C., The effects of northward IMF on the structure of the magnetosphere, *Geophys. Res. Lett.*, *12*, 839, 1985.

Yang, Y. S., R. W. Spiro, and R. A. Wolf, Generation of region-1 current by magnetospheric pressure gradients, *J. Geophys. Res.*, *94*, 223, 1994.

Zanetti, L. J., T. A. Potemra, T. Iijima, W. Baumjohann, and P. F. Bythrow, Ionospheric and birkeland current distributions for northward interplanetary magnetic field: Inferred polar convection, *J. Geophys. Res.*, *89*, 7453, 1984.

D. L. De Zeeuw, T. I. Gombosi, C. P. T. Groth, and P. Song, Space Physics Research Laboratory, University of Michigan, Ann Arbor, MI 48109-2143. (darrens@engin.umich.edu; tamas@umich.edu; groth@umich.edu; psong@umich.edu)

K. G. Powell, Department of Aerospace Engineering, University of Michigan, Ann Arbor, MI 48109-2140. (powell@engin.umich.edu)

(Received June 24, 1999; revised August 12, 1999; accepted August 19, 1999.)